Scanning Hall probe microscopy of vortex patterns in a superconducting microsquare

Taichiro Nishio,* Qinghua Chen, Werner Gillijns, Katrien De Keyser, Koen Vervaeke, and Victor V. Moshchalkov
INPAC-Institute for Nanoscale Physics and Chemistry, Katholieke Universiteit Leuven, Celestijnenlaan 200D, B-3001 Leuven, Belgium
(Received 22 May 2007; revised manuscript received 13 September 2007; published 23 January 2008)

We present direct observation of vortices confined to a superconducting 4×4 μm^2 square Pb film at 4.2 K with a high resolution scanning Hall probe microscope. Integrals of the magnetic field penetrating the square as a function of the applied field show that an applied-field dependence of vorticity L agrees with calculations based on the Ginzburg-Landau (GL) equation for a square sample geometry. From asymmetric field distribution of the confined magnetic flux, the locations of vortices on the square are inferred for vorticities $L=1-5$. The obtained vortex patterns are analogous with the calculations in the framework of the full GL equation for temperatures considerably lower than the superconducting transition temperature T_c.

DOI: 10.1103/PhysRevB.77.012502 PACS number(s): 74.78.Na, 74.78.Db

The geometry of superconducting samples (circular, triangular, square, etc.) fully defines the symmetry of the vortex patterns when the superconducting order parameter can be well described by the linearized version of the Ginzburg-Landau (GL) theory.[1–4] Among others, peculiar vortex patterns including a giant vortex[5,6] and an antivortex[3] can be realized in superconducting microstructures. The vortex patterns vary with the applied field, accompanying the oscillation of the superconducting transition temperature as a function of the magnetic field, $T_c(H)$. This oscillation has been observed in resistivity measurements and they give indirect experimental evidence for the formation of the symmetry-induced vortex patterns.[3,4] However, vortex visualization experiments have not given a sufficient direct evidence yet.

A few groups[7,8] have applied imaging techniques to visualization of vortex states in superconducting microstructures. Earlier, scanning supperconducting quantum interference device microscopy[7] has shown that vortex configurations in 30–50 μm sized Nb films with triangular and square forms are not exactly the same as the theoretical prediction. Bitter decoration results[8] indicate that vortices form shell structures[9] in 1–4 μm sized Nb disks, while triangular and square Nb films have no stable vortex configurations. Nb films have typically the strong pinning property, so that metastable states produced by strong pinning can easily destroy symmetry-induced vortex patterns. In addition, small coherence length $\xi(0)$ ($\sim$10 nm) of a Nb film might make it difficult to see stable vortex patterns because a theory requests that ξ should be above $\sim 0.1a$,[10] where a is a sample dimension: the stability of vortex patterns is expected above $\xi/a \sim 0.1$.

We now propose to study vortex configurations in superconducting Pb microstructures with a low pinning (the critical current j_c is considerably smaller than that of Nb films) and relatively large $\xi(0)$ [it has been reported to be 96 nm in bulk Pb (Ref. 11)]. In order to look at vortex configurations in the Pb sample, we use a scanning Hall probe microscope (SHPM) with a high spatial resolution. In this Brief Report, we present scanning Hall probe microscopy results for a 4×4 μm^2 Pb microsquare, in which vortex patterns inferred from multimonopole fits to flux images and its vorticity L are compared with calculations[3,10] based on the GL equation.

A Pb film of 50 nm in thickness was deposited on a Si substrate with a resist on which an array of squares was patterned by e-beam exposure. Subsequent lift-off procedures produced an array of 4×4 μm^2 square Pb films. We covered the films with a 50 nm thick Au film to make a coarse approach in a SHPM measurement after depositing a 20 nm thick Ge film on the Pb film to suppress the proximity effect[12] between Pb and Au films. Resistivity and magnetization measurements for a large reference plane film deposited under the same conditions give $T_c=7.2$ K, $\xi(0)=58$ nm, and the penetration depth $\lambda(0)=71$ nm, which were estimated from normal state resistivity ρ_0, the mean free path l, and the critical field $H_{c2}(T)$. A GL parameter κ of 1.2 shows that our Pb samples are in the type-II regime. The ratio between ξ and a is 0.022 at 4.2 K, which is higher than the values reported before for Nb microstructures[8] ($\sim$0.006 at 1.8 K).

We mounted the sample on a platform typical for a scanning tunneling microscopy technique. A Hall bar made up of $GaAs/Al_{0.3}Ga_{0.7}As$ was attached to a PZT5H piezoelectric scanning tube with a stick-slip coarse approach mechanism, which has a maximum scan range of $\sim$18 μm in the xy plane at 4.2 K. A Hall junction which is $\sim$1.0 μm ($=z$) away from the surface has dimensions of 1×1 μm^2, which yields a spatial resolution of about 0.85 μm.[13] A magnetic field sensitivity is $\sim 1.1\times10^{-3}$ $G/Hz^{1/2}$ at 77 K.[13] The whole assembly was put in a cryostat mounted on a vibration isolation platform with a double stage.

SHPM images of the flux in the square were taken on field cooling and subsequent field removal at 4.2 K. The Meissner effect observed as a square image after field cooling shows the position of the square on the substrate, so that basically we can know the location of the flux on the square by comparing the images of the flux and the square.

Figure 1(a) shows a SHPM image of the flux at 4.2 K and an applied field of 2.6 G. The trapped flux in the image has a width larger than an effective penetration depth[14] λ_{eff} (4.2 K) [$=2\lambda^2(4.2\text{ K})/d$, where d is a film thickness] of 0.48 μm because the distribution of the magnetic flux which comes out of a sample surface depends on the distance from the surface. In the case that $r^2+z^2 \gg \lambda_{eff}^2$, where $\mathbf{r}=(x,y)$ is the distance from the center of the flux, such as in our case, in general, the field distribution of a vortex can be approximated by a monopole model,[15]

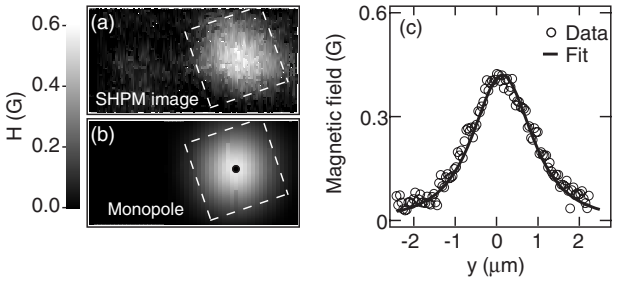

FIG. 1. (a) A SHPM image of the flux confined to the square Pb film at $T=4.2$ K and $H=2.6$ G. A scan area is 10×5 μm^2. (b) The result of the two dimensional (2D) monopole fit. The monopole position is shown as a black point. The broken lines show the shape of the square in (a) and (b). (c) The vertical sections of (a) the flux image and (b) the monopole image.

$$B_z(r,z) = \frac{\phi_0}{2\pi}\frac{z+\lambda_{eff}}{[r^2+(z+\lambda_{eff})^2]^{3/2}}, \tag{1}$$

where $B_z(r,z)$ and ϕ_0 are the magnetic field perpendicular to the surface and the flux quantum (20.7 G μm^2). As a result of the single monopole fitting to Fig. 1(a) involving a convolution with the size of the Hall junction, the flux image agrees well with the image of the monopole located at 0.12 ± 0.15 μm away from the center of the square, as shown in Figs. 1(b) and 1(c). The fit gives $z+\lambda_{eff}=1.51\pm0.10$ μm, which consistently results in $\lambda_{eff}\sim0.5$ μm. We have checked these values with those for other squares and have obtained similar results. This fitting procedure makes it possible to specify vortex locations on the square within errors.

We note that integrals of the magnetic field within 5 μm from the centers of the vortex and the monopole are 18.2 and 19.8 G μm^2, respectively, which are in good agreement [an integral for the monopole image in an infinite region gives the flux quantum (20.7 G μm^2)]. We define an effective flux quantum ϕ_1, which a single vortex has in our scan range, as 19.8 G μm^2.

Figure 2 shows the applied-field dependence of ϕ/ϕ_1 determined from the integrals taken within 5 μm from the center of vortex images at applied fields from 0 to 10.6 G. Integrated values change discontinuously with the applied field as a step function and the jumps roughly fall on ϕ_1, $2\phi_1$,…, and $5\phi_1$. It is natural to interpret these steps as changes in vorticity L with the applied field. In a large plane film or a bulk sample, the number of vortices increases when an amount of the applied flux through a superconductor reaches ϕ_0, $2\phi_0$,…: if the vortex entry in a microscopic superconductor behaved the same, L would increase at applied fields where the broken line crosses ϕ_0, $2\phi_0$,…, and $5\phi_0$ (Fig. 2). However, in the square, the increase of L does not follow this behavior: applied fields for vortex entry are about two times larger than in a large plane film. We have checked remnant fields inside our cryostat and added it to applied fields, so that the fact that the vortex entry fields are two times larger is not due to the remnant field.

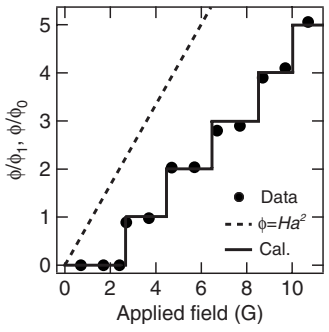

FIG. 2. Applied-field dependence of ϕ/ϕ_1 (solid points). The broken line shows an amount of the flux ϕ/ϕ_0 across an a^2 ($a=4$ μm) square area with the applied field (see text). The GL calculation for the vortex entry in the square sample is shown by solid lines.

According to the GL theory,[3] applied fields changing L depend on the lowest Landau level $E_{LLL}(H)$ of the GL equation. The $E_{LLL}(H)$ cusp's positions for the square give an applied-field dependence of L at 4.2 K shown as solid lines in Fig. 2, which is weakly dependent on temperature near T_c and almost independent at lower temperatures. The experimental data roughly fall on the solid lines. This agreement indicates that the sample boundary surely affects the vortex entry in our sample.

We now discuss some vortex images taken at higher applied fields [Figs. 3(a), 3(c), 3(e), and 3(g)]. We note that L's in those images have been already assigned by calculating the number of the flux from the integrals for the vortex images [L from 2 to 5 is assigned to Figs. 3(a), 3(c), 3(e), and 3(g), respectively]. They do not look like images of several ϕ_0 vortices though L's are larger than 1. It is tempting to suggest that these are giant-vortex images, but actually this is not the case here. We note that the field distribution of a single vortex in the square can be approximated by that of a monopole. It is reasonable to expect that fits using the multimonopole's field can reproduce those images in the same way. We attempt to fit the multimonopole's field to Figs. 3(a), 3(c), 3(e), and 3(g).

Figures 3(b), 3(d), 3(f), and 3(h) show results of the two dimensional (2D) multimonopole fits to data presented in Figs. 3(a), 3(c), 3(e), and 3(h), respectively. The fits were made assuming that the vortex images do not have contributions arising from a giant-vortex and a vortex-antivortex pair. The resultant $z+\lambda_{eff}$ values are 1.32 ± 0.05, 1.28 ± 0.11, 1.63 ± 0.05, and 1.50 ± 0.03 μm at $L=2$–5, respectively, which should be almost same because $z\sim1.0$ μm in each scan. The small difference between them may come from errors in a lift-off of the Hall probe z ($\sim\pm0.1$ μm). Experimental errors in vortex positions are within ±0.15 μm.

In Fig. 4, comparisons of the distances from the center of the square to contour lines of $H=0.44$ G ($L=1$), 1.0 G ($L=2$), 1.3 G ($L=3$), 2.2 G ($L=4$), and 3.6 G ($L=5$) between the observed SHPM images and the fits are displayed as a function of the angle measured counterclockwise, showing the accuracy in fitting. The peak positions denoted by broken lines indicate the direction in which a vortex is sitting, so that the number of the peaks implies the symmetry of the vortex patterns, though small differences in peak height be-

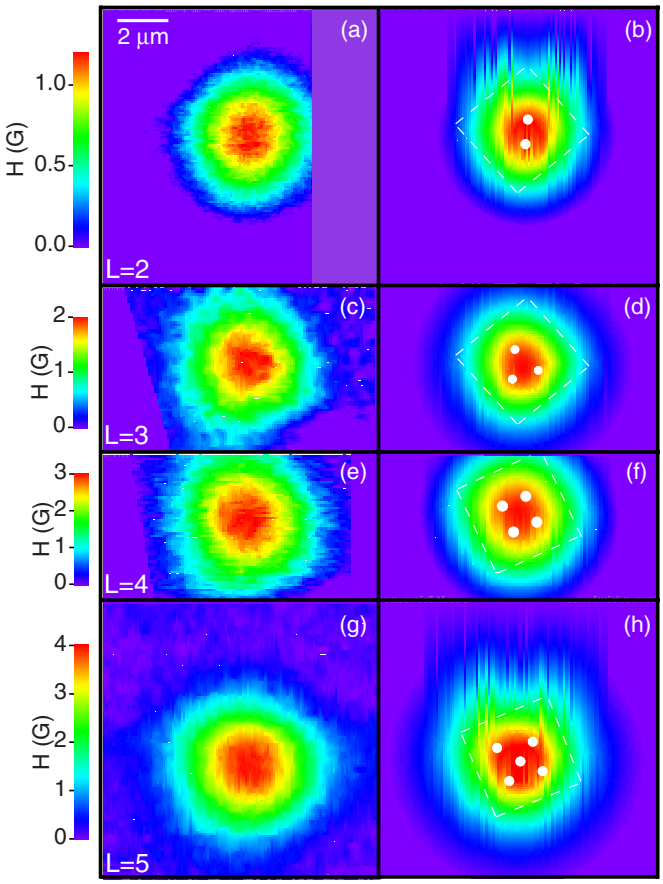

FIG. 3. (Color online) SHPM images of vortices in the square at applied fields of (a) 4.6 G, (c) 6.6 G, (e) 8.6 G, and (g) 10.6 G. [(b), (d), (f), and (h)] The results of the 2D monopole fits to (a), (c), (e), and (g), respectively. The broken lines denote the shape of the square. The locations of vortices are shown as white points, of which diameter corresponds to an experimental error.

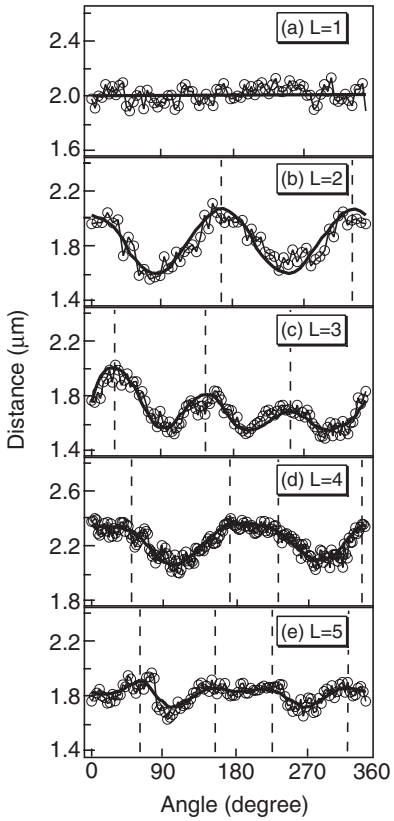

FIG. 4. The distances between the center of the square and contour lines as a function of the angle measured counterclockwise, starting with 0° at the top of the images for (a) $L=1$ in Fig. 1 and (b) $L=2$, (c) $L=3$, (d) $L=4$, and (e) $L=5$ in Fig. 3 (see text). The circle and the solid line are derived from the SHPM images and the 2D monopole fits in Fig. 3, respectively. The broken lines show the positions of the peaks in the fitting curves (see text).

tween peaks show that the symmetry is not perfect.

Let us now consider the implications of these experimental findings.

(1) $L=1$. In a calculation for $L=1$,[3] the central position of the square is energetically favorable when a vortex sits in the square. Figure 1(b) shows that a vortex is within the error from the center of the square.

(2) $L=2$. Calculations[10] show that the giant-vortex state persists below $a^2/\xi^2 \sim 50$ and above it a $2\phi_0$ giant vortex splits into two ϕ_0 vortices arranged along the diagonal. A fit of a single monopole with $2\phi_0$ does not reproduce the image in Fig. 3(a) well. The best fit shown in Fig. 3(b) indicates that vortices are arranged along the diagonal within the errors. This is reasonable because the vortex image was taken above the transition point between the giant-vortex and the ϕ_0 vortex state. The GL theory[3,16] predicts that vortices separated at the transition point move away from each other rapidly as temperature decreases. Our calculation[16] gives an intervortex distance of 1.4 μm at 4.2 K, which is close to an experimental value of 1.3 μm.

(3) $L=3$. It has been suggested that at the phase boundary $T_c(H)$, an antivortex is spontaneously formed at the center of the square with four vortices arranged along the diagonals below $a^2/\xi^2 \sim 50$ and above it three vortices form a triangle.[3,10] A fit of an antimonopole accompanying four monopoles does not reproduce the vortex image in Fig. 3(c). Triangular symmetry inferred in Fig. 3(d) is not inconsistent with the theory for $T \ll T_c$.

(4) $L=4$ and 5. The fits in Figs. 3(f) and 3(h) show that four vortices are located at the corners in $L=4$ and a vortex is located at the center with four vortices at the corners in $L=5$ within the errors, which is analogous to calculations[3] that it is energetically favorable that vortices are sitting at each corner in $L=4$ and, in addition to that, a vortex is located at the center in $L=5$.

According to comparisons with fitting results for other squares, the squares seem to possess equally those vortex patterns and each pattern does not change with an increase of the applied field which does not change L. The obtained vortex patterns, which could be also affected by the presence of pinning centers, are somewhat deformed in comparison with calculations; however, they are all fairly good symmetries of the predictions from the GL equation for $T \ll T_c$.

In summary, we have observed flux patterns in a 4×4 μm^2 square Pb film with a SHPM. An applied-field dependence of L we obtained agrees with the predictions of a

theory based on the GL equation with a square sample boundary. As a result of multimonopole fits to observed flux patterns, it is found that the inferred vortex patterns at 4.2 K for $L \leq 5$ are analogous to the predictions for $T \ll T_c$.

We acknowledge support from the Flemish FWO, the Belgian Interuniversity Attraction Poles (IUAP), the Research Fund K. U. Leuven (GOA), and the ESF-NES "Nanoscience and Engineering in Superconductivity" Programmes.

*taichiro.nishio@fys.kuleuven.be

[1] V. V. Moshchalkov, L. Gielen, C. Strunk, R. Jonckheere, X. Qiu, C. Van Haesendonck, and Y. Bruynseraede, Nature (London) **373**, 319 (1995).
[2] V. A. Schweigert, F. M. Peeters, and P. S. Deo, Phys. Rev. Lett. **81**, 2783 (1998).
[3] L. F. Chibotaru, A. Ceulemans, V. Bruyndoncx, and V. V. Moshchalkov, Nature (London) **408**, 833 (2000).
[4] L. F. Chibotaru, A. Ceulemans, V. Bruyndoncx, and V. V. Moshchalkov, Phys. Rev. Lett. **86**, 1323 (2001).
[5] D. Saint-James, Phys. Lett. **15**, 13 (1965).
[6] H. J. Fink and A. G. Presson, Phys. Rev. **151**, 219 (1966).
[7] T. Nishio, S. Okayasu, J. Suzuki, and K. Kadowaki, Physica C **412-414**, 379 (2004).
[8] I. V. Grigorieva, W. Escoffier, J. Richardson, L. Y. Vinnikov, S. Dubonos, and V. Oboznov, Phys. Rev. Lett. **96**, 077005 (2006).
[9] Y. E. Lozovik and E. A. Rakoch, Phys. Rev. B **57**, 1214 (1998).
[10] G. Teniers, Ph.D. thesis, K. U. Leuven, 2003.
[11] R. F. Gasparovic and W. L. McLean, Phys. Rev. B **2**, 2519 (1970).
[12] W. L. McMillan, Phys. Rev. **175**, 537 (1968).
[13] A. Oral, S. J. Bending, and H. Henini, J. Vac. Sci. Technol. B **14**, 1202 (1996).
[14] J. Pearl, Appl. Phys. Lett. **5**, 65 (1964).
[15] A. M. Chang, H. D. Hallen, L. Harriott, H. F. Hess, H. L. Kao, J. Kwo, R. E. Miller, R. Wolfe, J. van der Ziel, and T. Y. Chang, Appl. Phys. Lett. **61**, 1974 (1992).
[16] We calculate the full GL equation to derive the distribution of the superconducting order parameter in the square from 4.2 K to T_c on the basis of Ref. 17: $G=\int[\alpha|\Psi|^2+\Psi^\star\hat{L}\Psi+\beta|\Psi|^4]d\vec{r}$, where $\hat{L}=\left(-i\hbar\vec{\nabla}-\frac{2e}{c}\vec{A}\right)^2/2m^*$, α and β are the GL parameters, $\vec{A}$ is the vector potential, and Ψ is the order parameter. The boundary condition for a superconductor/vacuum interface can be written as $\left(\frac{\hbar\vec{\nabla}}{i}-\frac{2e}{c}\vec{A}\right)\Psi|_n=0$. When ξ(T) is larger than d, it is possible to expand Ψ into the solutions ϕ_i of the linearized GL equation $\hat{L}\phi_i=\epsilon_i\phi_i$: $\Psi=\Sigma c_i\phi_i$, where c_i is the complex expansion coefficient. Moreover, the free energy can be rewritten in a simple form, $G=\Sigma(\alpha+\epsilon)c_j^\star c_j+\frac{\beta}{2}A_{ij}^{kl}c_i^\star c_j^\star c_k c_l$, where $A_{ij}^{kl}=\int\phi_i^\star\phi_j^\star\phi_k\phi_l d\vec{r}$. We obtain the distribution in the square as well as the distance between vortices at $L=2$ by minimizing the free energy.
[17] L. F. Chibotaru, A. Ceulemans, G. Teniers, V. Bruyndoncx, and V. V. Moshchalkov, Eur. Phys. J. B **27**, 341 (2002).